ACS Photonics

Article

pubs.acs.org/journal/apchd5

Nanoparticle–Film Plasmon Ruler Interrogated with Transmission Visible Spectroscopy

Ryan T. Hill,*[,†] Klaudia M. Kozek,[†,⊥] Angus Hucknall,[†] David R. Smith,[‡,§] and Ashutosh Chilkoti[†,∥]

[†]Department of Biomedical Engineering, [‡]Department of Electrical and Computer Engineering, [§]Center for Metamaterials and Integrated Plasmonics, and [∥]Center for Biologically Inspired Materials and Material Systems, Duke University, Durham, North Carolina 27708, United States

Supporting Information

ABSTRACT: The widespread use of plasmonic nanorulers (PNRs) in sensing platforms has been plagued by technical challenges associated with the development of methods to fabricate precisely controlled nanostructures with high yield and characterize them with high throughput. We have previously shown that creating PNRs in a nanoparticle–film (NP–film) format enables the fabrication of an extremely large population of uniform PNRs with 100% yield using a self-assembly approach, which facilitates high-throughput PNR characterization using ensemble spectroscopic measurements and eliminates the need for expensive microscopy systems required by many other PNR platforms. We expand upon this prior work herein, showing that the NP–film PNR can be made compatible with aqueous sensing studies by adapting it for use in a transmission localized surface plasmon resonance spectroscopy format, where the coupled NP–film resonance responsible for the PNR signal is directly probed using an extinction measurement from a standard spectrophotometer. We designed slide holders that fit inside standard spectrophotometer cuvettes and position NP–film samples so that the coupled NP–film resonance can be detected in a collinear optical configuration. Once the NP–film PNR samples are cuvette-compatible, it is straightforward to calibrate the PNR in aqueous solution and use it to characterize dynamic, angstrom-scale distance changes resulting from pH-induced swelling of polyelectrolyte (PE) spacer layers as thin as 1 PE layer and also of a self-assembled monolayer of an amine-terminated alkanethiol. This development is an important step toward making PNR sensors more user-friendly and encouraging their widespread use in various sensing schemes.

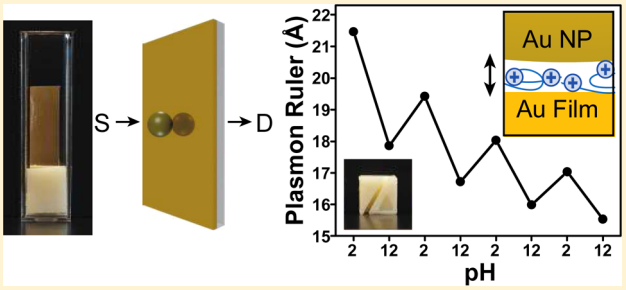

KEYWORDS: *plasmonics, 3D printing, localized surface plasmon resonance, plasmon coupling, plasmon ruler, sensor*

Plasmonic nanorulers (PNRs)—rulers that transduce distance via a distance-dependent spectral shift of a coupled plasmon resonance—have been in development for at least a decade.[1−7] However, their widespread incorporation into robust sensing platforms has been impeded by technical challenges associated with precisely defining, modulating, and detecting nanoscale separation distances between two surface plasmon-supporting structures. Nevertheless, the development of PNRs for sensing remains attractive due to their exquisite, angstrom-scale sensitivity to distance.[8] This distance sensitivity can be exploited in a manner similar to Förster resonance energy transfer (FRET)-based sensors, but in the case of PNRs the distance sensitivity extends over a longer range[2] and signal transduction is more stable since it is not susceptible to photobleaching.[9,10]

The use of PNRs in sensing has been hindered by the lack of a viable strategy to create a PNR platform that is both efficient—in fabrication and characterization—and robust. PNR sensors in the form of colloidal nanoparticle (NP) assemblies[11,12] are efficient from the standpoint of high-throughput signal transduction, because many PNRs can be interrogated with a single spectroscopic measurement, and also from the standpoint of fabrication since the process relies on self-assembly. However, the main disadvantage of colloidal PNRs is that they are not robust. The stability of colloids in suspension is extremely sensitive to salt concentration and other solutes such as proteins and DNA, and so it is challenging to use colloidal PNR sensors in direct contact with biological fluids such as blood or serum.

A more robust method to create PNR sensors is to immobilize them onto a substrate[2,3,7,13−15] to minimize the risk of colloidal flocculation during a sensing experiment. Indeed, this strategy has enabled PNRs to sensitively detect biomolecules, even in complex media such as serum.[14,15] However, a major drawback that prevents surface-based NP dimer PNR sensors from being widely used is the low efficiency of their synthesis. As a result, their characterization is often cumbersome and time-consuming, as it must be done one PNR at a time using a microscope to identify single PNRs among a large background population of plasmon resonant NPs that are not PNRs.

Received: May 28, 2014
Published: September 11, 2014

We recently demonstrated a surface-based version of the PNR where distances can be measured using plasmon coupling between gold NPs and a thin gold film (NP−film).[8,16−18] Here, NP−film PNRs are created with 100% yield by simply immobilizing NPs to the gold film with an intervening molecular spacer that is typically deposited on the gold film before NP deposition. To understand the optical properties of film-coupled NPs, the gold film (analogous to a reflecting mirror) can be conceptually replaced by an image dipole; light scattered from a film-coupled NP thus resembles that scattered from two "real" metal NPs that are physically separated in space.[18] Because the NP−film PNR requires only chemically synthesized gold NPs to be tethered to a bulk gold film by a molecular linker, and because these NPs are easy to reproducibly synthesize with controlled sizes and shapes, the NP−film PNR allows one to efficiently create, identify, and interrogate millions of identical molecular rulers. Since the NP−film PNR fabrication process results in such a uniform population of PNRs, it is possible to simultaneously interrogate an ensemble of PNRs with a single optical measurement, as opposed to having to identify and characterize the rulers one-by-one, as is the case for immobilized NP dimer PNRs. The significance of ensemble measurements is that they dramatically increase the signal-to-noise ratio, analytical precision and accuracy, and throughput of the PNR sensor.[8] The high efficiency of the NP−film format combined with the robust nature of the surface-bound PNR platforms suggests that the NP−film PNR is well suited for incorporation into more user-friendly PNR sensing schemes.

The NP−film PNR still faces a significant challenge to be useful for biosensing, which is the development of a strategy to make high-throughput PNR measurements in an aqueous environment. This is a nontrivial challenge because a reflective, metallic film is an integral part of the NP−film PNR sensing platform. Initial configuration of the platform[18] assumed the PNR to be in air (dry state) and interrogated using reflected dark field microscopy, which does not easily accommodate hydrated NP−film samples due to the fact that, at least for the case of spherical NPs, NP−film PNRs must be illuminated at an oblique angle so as excite the coupled NP−film resonance. In reflected dark field imaging the numerical aperture (NA) of the objective determines the illumination angle, and so high-NA objectives provide better NP−film PNR excitation. However, imaging through a water−air or glass−air interface with high-NA reflected dark field objectives, which are not available as immersion objectives, usually creates high background scattering that degrades the NP−film PNR signal. To combat this problem, we explored the use of totally internally reflected (TIR) white light illumination coupled into the back side of a glass/gold film substrate using a prism, which facilitates the use of liquid cells on top of the gold film surface.[17,18] This approach was successful to some degree, but it is spectrally complicated due to the strong presence of the gold film SPR, which is also excited in the TIR configuration.

The focus of this paper is to demonstrate a new and experimentally convenient method to make high-throughput NP−film PNR measurements in water using more standard laboratory equipment. We show that when semitransparent gold films (30 nm thick) are used to create the NP−film PNRs, they can be characterized in a transmitted light configuration, where the ensemble NP−film extinction is measured using a standard UV−vis spectrophotometer from an NP−film PNR sample inserted into a cuvette. This measurement configuration is similar to the previously demonstrated transmission localized surface plasmon resonance spectroscopy (T-LSPR, also called T-SPR) configuration,[19−24] where the extinction of a population of plasmon resonant NPs immobilized onto a transparent substrate is measured by a spectrophotometer. The advantages of this technique are that (1) the instrumentation required is standard equipment, as spectrophotometers are relatively inexpensive and widely used; (2) the spectroscopic measurement is of an ensemble of sensors, which increases accuracy, precision, and throughput; and (3) the configuration is amenable to hydrated sensing experiments given the use of a standard spectrophotometry cuvette as a sample container and a transmitted light optical configuration. We present herein a characterization and distance calibration of the hydrated NP−film PNR in T-LSPR mode and then demonstrate that the NP−film T-LSPR PNR can be used to detect dynamic, angstrom-scale thickness changes in molecular spacer layers in response to changes in solution pH. This demonstration should prove to be an important step toward the incorporation of PNRs into useful sensing platforms that require aqueous environments or into those where a collinear optical path is favorable over a reflected geometry.

RESULTS AND DISCUSSION

Excitation of the coupled NP−film resonance depends on the illuminating beam having a polarization component that aligns along the axis normal to the surface of the gold film. We and others have shown this previously by demonstrating that NP−film reflectivity and surface-enhanced Raman measurements reveal strong interaction with p-polarized incident light and minimal interaction with s-polarized light.[8,17,25−27] Thus, the key to exciting the coupled NP−film resonance using a transmitted, collinear optical extinction measurement is to place the sample at an angle relative to the light path so that the propagating beam has a polarization component that contributes to p-polarization and is capable of exciting the NP−film dipole (Figure 1). If the NP−film axis, which is normal to the film surface, is parallel to the axis of the propagating beam (Figure 1A), then the illumination is effectively s-polarized and is incapable of exciting the NP−film resonance because the axes of the film-coupled NP dipoles are all orthogonal to the electric field component of the beam. As soon as the NP−film sample is rotated such that the NP−film axis is not parallel to the axis of the propagating beam (Figure 1B), then the electric field component of the beam can contribute to p-polarized illumination of the NP−film sample, hence exciting the NP−film resonant dipoles.

We demonstrate the effect of illumination angle on the NP−film LSPR measurement in both reflectivity and transmission measurements. Reflectivity was measured using a variable-angle spectroscopic ellipsometer (VASE), and transmission measurements were made using a UV−vis spectrophotometer and custom slide holders (Figure 2A−C) to support NP−film samples inside standard, 1 cm spectrophotometer cuvettes such that the angular orientation of the sample could be controlled relative to the incident light. With these mounts, we were able to make NP−film LSPR extinction measurements at a series of angles to compare the PNR response seen from reflectivity and transmission illumination modes.

We created an NP−film sample with a 30 nm gold film, a single polyelectrolyte (PE) spacer layer (poly(allylamine) hydrochloride, PAH), and 60 nm gold NPs at a surface coverage of ∼5 NPs per μm^2, which produced an NP−film

dx.doi.org/10.1021/ph500190q | ACS Photonics 2014, 1, 974−984

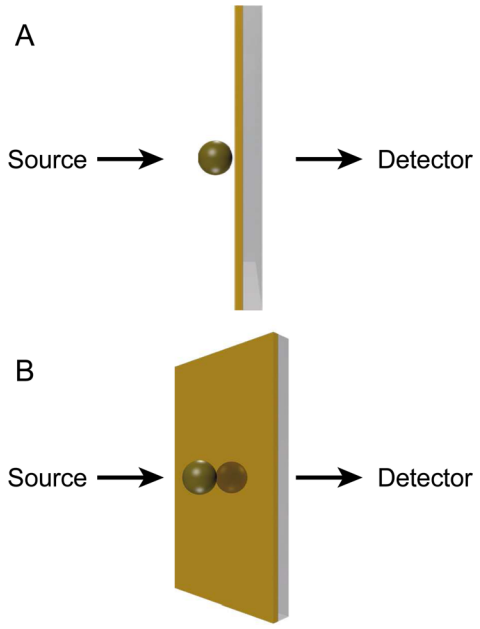

Figure 1. Excitation of the coupled nanoparticle−film (NP−film) resonance depends on the illuminating beam having p-polarization or a polarization dipole component that aligns along the axis defined by the NPs and film. In a collinear transmitted light configuration using unpolarized light, the illumination of a NP−film sample at normal incidence results effectively in s-polarized illumination and is incapable of exciting the coupled NP−film resonance because all polarization dipoles in the propagating beam are orthogonal to the NP−film resonant dipole axis (A). If the NP−film sample is placed at an angle relative to the illumination path, then the NP−film resonant dipole can be excited because some fraction of the propagating beam contributes to p-polarization (B).

separation distance of <1 nm so as to obtain a red-shifted, coupled NP−film LSPR. A reflected dark field image and corresponding scanning electron micrograph showing NP surface coverage of such a sample can be seen in the Supporting Information and shows that the surface coverage of the NPs is high enough that single NPs are not individually resolved in the optical image, but still low enough that lateral plasmonic coupling between NPs is minimal.[17]

Figure 2D shows the extinction of the dry NP−film sample measured in reflectivity mode using p-polarized light and with illumination angle varying from 45° to 70° relative to the normal to the gold film surface. In each case, the sample spectrum is normalized to a blank spectrum of a gold film containing 1 PE layer and no immobilized NPs. The general trend in this data is that the NP−film extinction peak intensifies as the angle is increased. There are two reasons for this trend in the data. The first reason is that as the angle of illumination increases, the number of film-coupled NPs interrogated by the beam increases due to the elongation of the illuminated spot on the substrate. The second and more significant reason for the trend in the data is that as the illumination angle increases, the polarization of the excitatory electric field in the illumination beam is better aligned with the NP−film resonant dipole, which is aligned along the axis normal to the surface of the gold film.

Using the same NP−film sample with a 1-PE spacer layer, we collected NP−film extinction spectra in T-LSPR mode using a spectrophotometer with the samples inserted into the custom slide holders contained inside of water-filled cuvettes, which positioned the sample at various illumination angles (Figure 2E). Here again, the sample spectra were baseline corrected to blank spectra collected at each angle from samples containing 30 nm gold film, 1 PE layer, and no immobilized NPs. We used unpolarized light from the spectrophotometer in this case so as to make the T-LSPR measurement in the simplest possible optical configuration, though we note that a polarizer can be easily added to the optical path. When the sample was positioned such that the illumination angle was at 0° relative to the gold film surface normal (i.e., such that the NP−film resonant dipoles are parallel to the propagating beam), an illumination angle that was not possible in reflectivity mode due to instrument limitations, the red-shifted NP−film resonance was not apparent at all in the spectrum. There was, however, a weak resonance peak located at ∼545 nm, which we attribute to a slight excitation of the uncoupled 60 nm NP LSPR. The absence of the coupled NP−film resonance is due to the illumination in this case being effectively s-polarized and incapable of exciting the coupled NP−film resonance. It is not until the illumination angle increases that the red-shifted NP−film coupled resonance appears at ∼740 nm. The NP−film resonance in this case is red-shifted relative to the reflectivity data because the T-LSPR data were taken in water. We note that in the T-LSPR spectra we collected throughout these experiments, it was not uncommon for the overall baseline signal levels to vary slightly from sample to sample. We attribute this to a combination of instrument baseline drift and the slight variation in sample placement that is caused by the tolerance of the 3D printed slide holders. Thus, the increasing NP−film extinction peak with increasing illumination angle presented in Figure 2E becomes more apparent and similar to that seen in the reflectivity data (Figure 2D), after the spectra are baseline adjusted to a feature common to all the spectra, which we chose to be the average extinction value of the noisy region between 850 and 900 nm that defines the base of the long-wavelength side of the NP−film extinction peak.

The data presented in Figure 2 show that the ability to excite the coupled NP−film resonance in transmission mode is crucially dependent on the illumination angle being such that the axis of the coupled NP−film dipole is not parallel to the propagating illumination beam, so that the illumination contributes to p-polarized excitation. It is interesting to note that similar T-LSPR measurements have been made on NP−film samples,[28−32] and in some cases a distinct, coupled NP−film resonance was not observed. In some instances,[28,31] the films were extremely thin (4 nm) and described as gold nanoislands, which were being coupled to a dense, close-packed network of very small NPs (12−13 nm diameter) entrapped within polymer brushes to make sensitive plasmonic pH sensors. Since the film in this case was likely not continuous and the NPs likely penetrate to some degree into the polymer brush films to form a complex plasmonically coupled 3D network,[33] the coupled resonant dipoles—both NP−NP coupling and NP−nanoisland coupling—responsible for the sensor signal were likely varying dramatically in orientation. We presume that the apparent shift in the native LSPR of the Au nanoislands with the addition of nearby NPs into the polymer brushes was measured with some degree of NP−NP and NP−nanoisland LSPR coupling from resonant dipoles that could be excited by s-polarized illumination at normal incidence. Polymer swelling was detected by a plamson shift from the ensemble, networked NP assembly as the polymer brushes changed configuration.

dx.doi.org/10.1021/ph500190q | ACS Photonics 2014, 1, 974−984

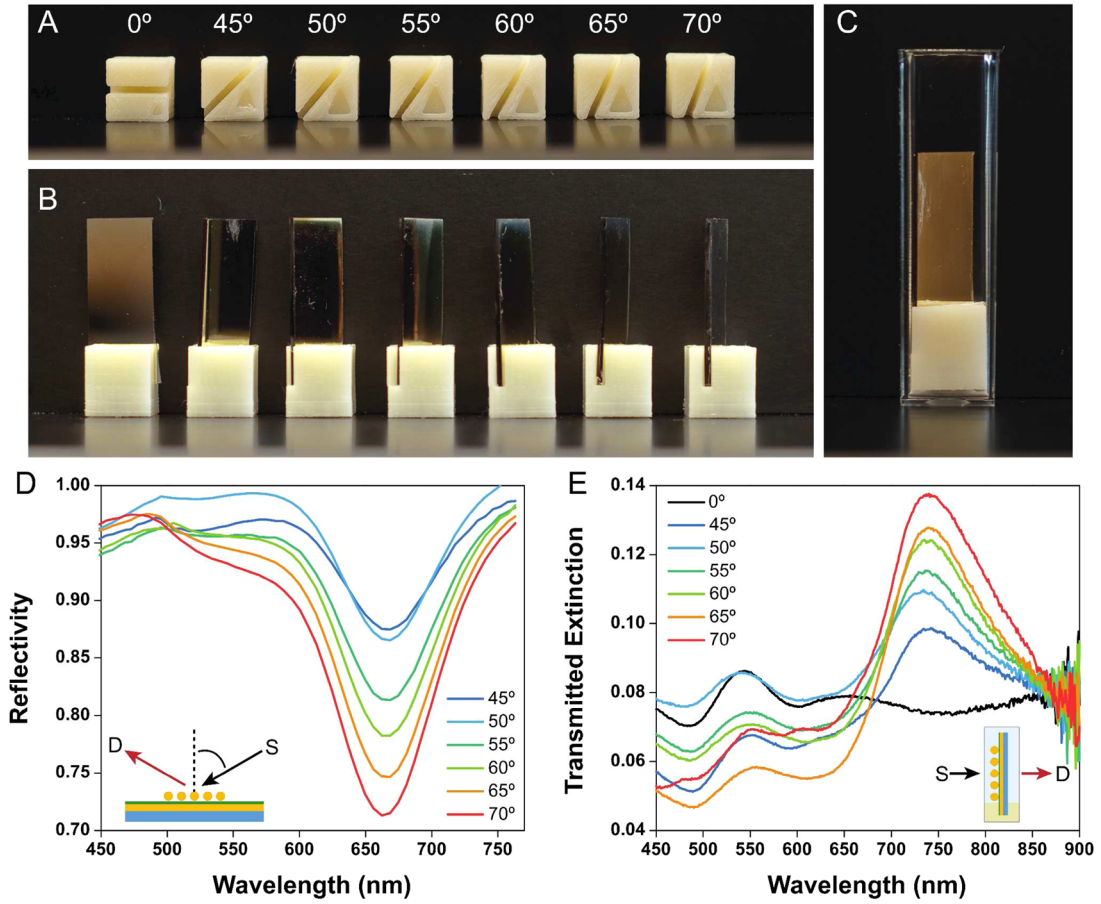

Figure 2. To demonstrate the effect of illumination angle on transmission localized surface plasmon resonance (T-LSPR) spectroscopy of a coupled nanoparticle−film (NP−film) sample, we designed slide holders (A, B) that fit into standard 1 cm spectrophotometer cuvettes (C). (D) Reflectivity spectra at various p-polarized illumination angles relative to the normal to the gold film of a dry sample composed of 60 nm gold NPs separated from 30 nm thick gold film (supported by a glass microscope slide) by 1 polyelectrolyte (PE) spacer layer, which positioned the NPs <1 nm away from the gold film. The coupled NP−film resonance increases in intensity as the illumination angle increases. The same sample is characterized in water using T-LSPR spectroscopy (unpolarized illumination) and the slide holders in A and B. (E) Similar to the reflectivity measurements in D, the coupled NP−film resonance increases with increasing illumination angle in the transmitted configuration. The coupled NP−film resonance is not apparent in the spectrum when the illumination angle is 0°. The spectra in E are baseline corrected so that they all have the same average absorbance value in the noisy region between 850 and 900 nm that defines the base of the long-wavelength side of the NP−film resonance peak. Spectra in D and E are normalized/baseline corrected to a blank spectrum taken of a gold film sample containing the PE spacer layer and no immobilized NPs. Insets in D and E depict the respective detection modes (S: source, D: detector).

In systems where the coupled LSPR dipoles vary in orientation, it is difficult to correlate the plasmon shifts observed to precise changes in the coupled LSPR separation distance, which complicates calibration of the PNR and hinders the ability to perform PNR measurements where distance changes are measured. These systems work well for detecting polymer swelling, but they depend on the ability to form close-packed NP networks, which is aided by the use of NP multilayers or 3D branched polymer brushes containing many NP binding sites on each brush. They would likely suffer from lack of signal in cases where a molecular layer binding NPs to film does not promote the formation of an immobilized high-density, close-packed NP network (e.g., a monolayer of biomolecules designed to bind 1 NP per molecule) due to the lack of coupled resonant dipoles excitable by s-polarized illumination at a 0° illumination angle.

These previous NP−film T-LSPR studies are drastically different from the NP−film system presented in this paper, where much larger, 60 nm NPs are used at much lower film surface coverage (~5 NPs per μm^2), and all of the coupled NP−film resonant dipoles have the same orientation (aligned normal to the gold film surface), excitable by p-polarized illumination. The results we see in our NP−film T-LSPR measurements are most similar to those observed by Okamoto and Yamaguchi[32] in an early characterization of the plasmonic coupling between gold NPs of various sizes and 25 nm thick gold film, where they observed distinct, coupled NP−film resonances in addition to native NP LSPRs with increasing T-LSPR illumination angle and p-polarized illumination. In such a system where the film-coupled NPs are all separated from the underlying continuous film by a uniform separation distance, it is straightforward to correlate shifts in the coupled NP−film LSPR to changes in the NP−film separation distance using a similar approach to our previous reports on NP−film PNRs.[8,16−18] In this NP−film system, the coupled resonance responsible for PNR signal transduction arises from the coupling of single NPs to the underlying film, with minimal contribution from lateral NP−NP coupling,[17] and hence it will not suffer from the use of molecular spacer layers that do not promote dense, close-packed NP immobilization.

dx.doi.org/10.1021/ph500190q | ACS Photonics 2014, 1, 974−984

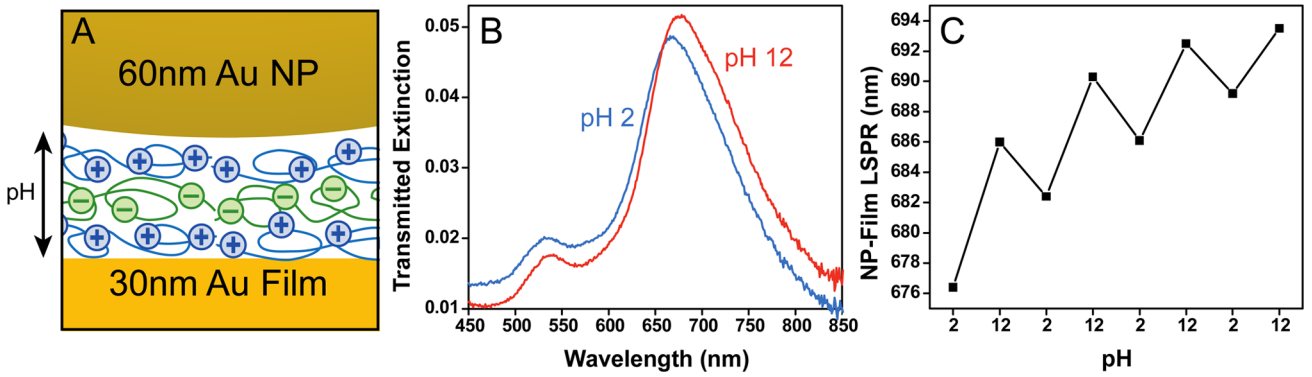

Figure 3. (A) A nanoparticle−film (NP−film) plasmon nanoruler (PNR) is used in transmission localized surface plasmon resonance spectroscopy (T-LSPR, 60° illumination angle) mode to characterize pH-induced swelling of a molecular spacer layer composed of 3 polyelectrolyte (PE) layers. (B) Spectra show the coupled NP−film LSPR blue-shifted by incubation at pH 2, suggesting that the 60 nm gold NPs have been pushed away from the underlying 30 nm gold film because the PE layer is in a swollen state. The NP−film LSPR red shifts when the sample is immersed in pH 12 solution, suggesting PE layer deswelling. (C) The NP−film LSPR peak centroid is plotted over the course of 8 pH switches, indicating semireversible pH-induced layer swelling. The data suggest that the PE layer experiences a net contraction after 8 pH switches, each of which consisted of a 30 min incubation time at the respective pH.

We next used the NP−film PNR in the T-LSPR configuration to interrogate small, dynamic molecular conformational changes by measuring the actuation of molecular spacer layers in response to solution pH. It has been shown previously that PE multilayers containing at least one weak PE, such as PAH, will swell and deswell in response to solution pH changes[34−37] because of protonation and deprotonation as a function of solution pH. While this swelling behavior has been shown previously using PE multilayers consisting of many bilayers, we show here how the NP−film PNR can be used to probe this actuation using only 1−3 PE layers (i.e., 0.5−1.5 bilayers), which highlights the unique ability of the NP−film PNR to sense distance changes from very thin molecular layers.

Figure 3 shows the NP−film PNR T-LSPR response from a pH swelling experiment in which we observed the actuation of a 3-PE layer (3L) sample over eight pH switches. We used layer-by-layer (LBL) deposition of oppositely charged PEs,[38,39] PAH, and polystyrenesulfonate (PSS), with PAH being the initial and terminal layers and also the weak PE that is susceptible to protonation with a change in pH. For this initial experiment, we deposited all three layers (Figure 3A) from solutions containing 3 mM of the PE (with respect to the monomer molecular weight) and 1 M NaCl dissolved in ultrapure water and made no attempt to adjust the pH of the deposition solutions.

Figure 3B shows representative NP−film T-LSPR data at each pH value. The NP−film coupled resonance, which is the strong peak between 650 and 700 nm, red shifts when the pH is switched from 2 to 12. This implies that at pH 2 the NPs on top of the 3L sample are further away from the film, because the PE multilayer is swollen, and that at pH 12 the NPs are closer to the film because the PE multilayer has contracted. This swelling trend is consistent with previous studies using multiple PE bilayers.[34,35] Once the NP−film LSPR peak location is plotted versus pH (Figure 3C), we see that there is a semireversible trend in the peak shift throughout the eight pH cycles. In the initial cycle, the switch from pH 2 to 12 results in a larger red shift than the blue shift that occurs when the pH is switched back from 12 to 2. This trend is consistent throughout the remainder of the cycles and implies that the 3L multilayer experienced a net contraction over the eight successive pH cycles.

To correlate the NP−film LSPR peak shifts we observed during the pH switches with changes in the molecular spacer layer thickness, we conducted an NP−film PNR distance calibration study similar to those we have demonstrated previously[8,17] with the exception that this study was done in aqueous solution using both reflectivity (Supporting Information) and T-LSPR NP−film extinction measurements. In the past we have only been able to perform this distance calibration of the NP−film PNR in the dry state, using either reflected dark field scattering or reflectivity extinction measurements. We created a series of NP−film samples with PE spacer layers of increasing thickness using LBL deposition of PEs. We used *in situ* ellipsometry to estimate the thicknesses of the hydrated PE spacer layers (Supporting Information), which are plotted along with the hydrated NP−film T-LSPR data to create a calibration curve.

The NP−film T-LSPR data from the calibration study done in water is shown in Figure 4. Similar data from both hydrated and dry PE layers in reflectivity and transmission modes are shown in the Supporting Information. We were able to identify a distinct NP−film coupled resonance in the T-LSPR extinction spectra (Figure 4A) for the NP−film samples with spacer layers extending out to 15 PE layers, which corresponded to a 34 nm separation distance between the NPs and film. Spectra from the 7L, 9L, and 11L ("*n*L" where "*n*" is the number of layers) NP−film samples produced oddly shaped NP−film extinction peaks, which we attribute to a spectral mixing effect between the uncoupled 60 nm NP LSPR and the coupled NP−film LSPR. Interestingly, this spectral mixing effect was not as apparent in the data taken in reflectivity mode or in the dry T-LSPR data (see Supporting Information for more discussion). We were able to minimize the effect of these features by inserting an inexpensive linear polarizer sheet into the spectrophotomer light path so as to deliver only p-polarized illumination to the NP−film samples, which preferentially excites the coupled NP−film resonance and, hence, produces more accurate NP−film LSPR peak positions to use for the distance calibration. We did not use the polarizer for the studies presented in Figure 3 or 5, because the use of the polarizer does not significantly alter the peak location for thin NP−film spacer layers such as the ones used in these studies (Supporting Information).

dx.doi.org/10.1021/ph500190q | *ACS Photonics* 2014, 1, 974−984

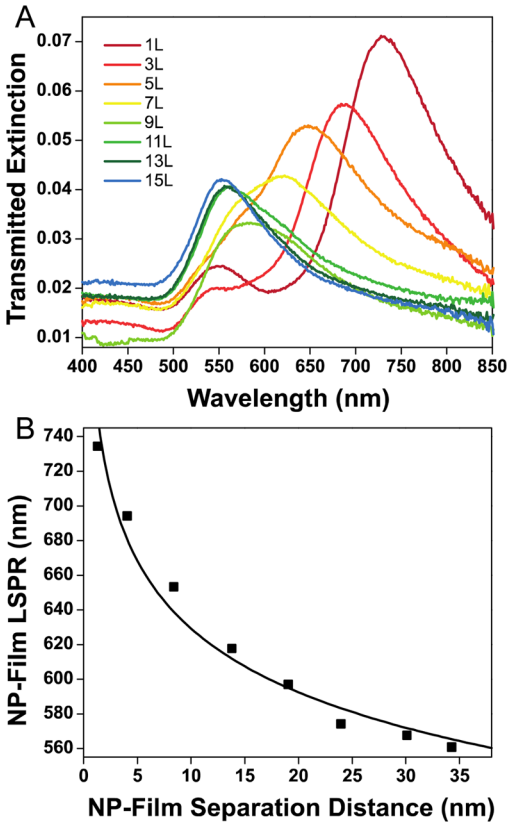

Figure 4. Nanoparticle–film (NP–film) plasmon nanoruler (PNR) transmission localized surface plasmon (T-LSPR) spectroscopy response using 60 nm Au NPs and 30 nm Au film was calibrated in water by creating NP–film samples using polyelectrolyte (PE) spacer layers with increasing thickness. (A) T-LSPR spectra (60° illumination angle, p-polarized) show the NP–film extinction spectra using PE spacer layers varying in thickness from 1 to 15 layers. The coupled NP–film LSPR blue shifts with increasing number of spacer layers. (B) The NP–film LSPR peak position is plotted versus NP–film separation distance, which is set by the PE spacer layer thickness, and shows the expected nonlinear blue shift of the NP–film LSPR with increasing NP–film separation distance. These data were fitted to a power law function (line plotted in B) and serve as a calibration curve for the NP–film PNR interrogated by T-LSPR spectroscopy.

Figure 4B shows the coupled NP–film LSPR peak position, as determined by calculating the centroid of the top 50% of the peaks, plotted against the NP–film separation distance, which shows the expected nonlinear blue-shifting LSPR trend with distance. We fitted these data to a power law function[8,17,40] by performing a linear regression (R^2 = 0.972 49) of the data plotted on a log–log scale (Supporting Information). These regression data for the T-LSPR data were used as a calibration curve to estimate dynamic changes in thickness from hydrated molecular layers in T-LSPR mode. The calibration curve determined from the fitting procedure was $y = 768.635x^{-0.08692}$ and is shown as a solid line in Figure 4B.

With the NP–film PNR T-LSPR calibration curve as reference to convert wavelength shifts in the NP–film LSPR to changes in distance, we used the NP–film PNR to compare the pH-induced swelling behavior of molecular spacer layers that differ in thickness and fabrication conditions. It has been suggested previously that the swelling behavior and thickness of PE multilayers are affected by the pH and ionic strength of the deposition solution.[35−37,41] We used the NP–film PNR to

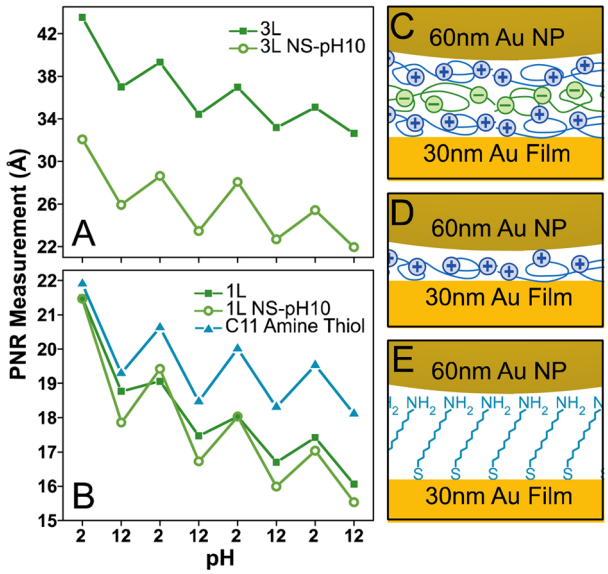

Figure 5. A nanoparticle–film (NP–film) plasmon nanoruler (PNR) was used to investigate the pH-induced swelling behavior of different molecular spacer layers. The parameter "PNR measurement", which is determined by converting the NP–film LSPR peak positions to NP–film separation distance using the calibration curve determined in Figure 4B, is plotted against pH for each spacer layer. Swelling of polyelectrolyte (PE) spacer layers fabricated in the presence of 1 M NaCl (dark green squares) and also without NaCl and with pH adjusted to pH 10 (designated as "NS-pH10", light green open circles) was compared. The 3 PE layer samples ("3L", C) show differing initial thicknesses and similar semireversible pH-induced swelling behavior (A). Both 1L (D) samples have similar initial thickness values and showed qualitatively similar swelling to the 3L samples (B). The NS-pH10 samples on average show a higher degree of swelling and deswelling relative to the same layers fabricated from solutions containing 1 M NaCl. A self-assembled monolayer of an 11-carbon amine-terminated thiol (C11 amine thiol, E) also demonstrated pH-induced swelling behavior (B, blue triangles).

investigate the pH swelling behavior of very thin PE layers, consisting of 3 PE layers (Figure 5C) and only 1 PE layer (Figure 5D). For both PE layer thicknesses, we also compared the swelling behavior of layers deposited from PE solutions containing 1 M NaCl in ultrapure water with those deposited from solutions that contained no additional NaCl and were adjusted to be pH 10, which is above the pK_a of PAH (pK_a ~9;[37] these layers are designated "NS-pH10", where "NS" stands for "no salt"). Each of the layers produced distinct dry ellipsometric thicknesses and corresponding NP–film LSPR peak positions after NP deposition: 24.7 Å and 612.9 nm for 3L, 20.1 Å and 623.9 nm for 3L NS-pH10, 3.8 Å and 654.3 nm for 1L, and 5.0 Å and 654.8 nm for 1L NS-pH10. The 3L samples showed a difference in thickness between the two deposition conditions, as indicated by the ellipsometric thickness and by the NP–film LSPR position. This observation is supported by previous studies showing that PE layers generally form thicker layers when deposited from solutions containing higher salt concentration.[41] Though the 1L samples showed a slight thickness variation (1.2 Å) in the ellipsometry data, the dry NP–film PNR LSPR peak positions differ only by 0.5 nm (corresponding roughly to 0.1 Å in thickness using the dry NP–film PNR sensitivity determined in Hill et al.[8]), which suggests that these 1L layers are quite similar in thickness. This discrepancy between the ellipsometry and PNR data is not

dx.doi.org/10.1021/ph500190q | ACS Photonics 2014, 1, 974−984

surprising, as we have found that our ellipsometric thickness values below ∼10 Å are not as accurate due to inherent limitations of ellipsometry.[8]

A summary of the pH-induced swelling of the multiple layers characterized by the NP−film PNR in T-LSPR mode is shown in Figure 5A and B. The PNR measurement was determined by tracking the coupled NP−film LSPR peak position for each layer type at each pH and then using the calibration curve generated by our calibration study (Figure 4B) to convert the peak positions to NP−film separation distances, which is designated as "PNR measurement". These data are from hydrated NP−film samples, and even so, the thickness trends we observed from the dry layers discussed above are also observed for the hydrated layers. The 3L sample fabricated in the non-pH-adjusted solutions containing salt was significantly thicker than the 3L NS-pH10 sample, both initially when immersed in pH 2 solution and throughout the pH cycles. Both 1L samples also had similar thicknesses initially at the first pH 2 measurement. Also, similar to the data from Figure 3, all layers demonstrated semireversible swelling such that after the 8 pH incubations all layers appeared to have experienced a net contraction relative to their initial thickness as measured at pH 2. We note that we have cycled a 1L sample through 16 pH switches over the course of 2 days and observed that the net layer contraction over successive pH cycles seems to approach an asymptotic limit after many pH cycles (Supporting Information).

A striking feature that is consistent throughout all of the PE spacer layer pH data in Figure 5 is that the NS-pH10 layers showed increased deswelling and swelling throughout the pH cycles relative to the layers that were deposited from solutions containing salt and ultrapure water that was not pH adjusted. The average deswelling and swelling between each pH switch for the 3L sample in terms of layer thickness were 4.4 Å (deswelling) and 2.3 Å (swelling), respectively, whereas the same figures for the 3L NS-pH10 sample were 5.0 Å (deswelling) and 3.4 Å (swelling). For the 1L samples, the averages were 1.8 Å (deswelling) and 0.5 Å (swelling) for the 1L sample and 2.5 Å (deswelling) and 1.3 Å (swelling) for the 1L NS-pH10 sample. The 3L NS-pH10 samples experienced 14% more deswelling and 48% more swelling relative to the 3L samples, and the 1L NS-pH10 samples experienced 41% more deswelling and 152% more swelling relative to the 1L samples.

Further study is required to firmly establish the trends in PE layer swelling observed from these NP−film PNR experiments and also to elucidate the effect, if any, of the NP stabilizing ligand (citrate) on the PNR response to pH changes. Nevertheless, the trends presented here qualitatively support those seen from previous studies showing pH-induced swelling of PE layers.[34,35] It has been shown before that PE multilayers containing PAH and PSS show exaggerated pH-induced swelling when the multilayers are assembled from alkaline solutions near the pK_a of PAH.[35−37] This is likely due to the increased incorporation of free amines into the PE multilayers, which creates a large amount of electrostatic repulsion when the pH is reduced to the point that all amines become protonated and positively charged. However, in contrast to previous reports,[35−37] our data suggest that the PE layers fabricated from relatively acidic solutions that were not pH adjusted to 10 are also capable of pH-induced swelling. We note here that the relatively acidic fabrication solutions used in this study also contained 1 M NaCl, whereas the pH < 10 fabrication solutions in the previous studies did not.

We also tested the susceptibility of an amine-terminated 11-carbon alkanethiol (C11 amine thiol) self-assembled monolayer (SAM) to pH-induced changes in NP−film separation distance using the NP−film PNR in T-LSPR mode (Figure 5E). The PNR data report a surprising degree of actuation (Figure 5B, blue triangles), as we expected the amine thiol SAM spacer layer to be more well-ordered and less prone to electrostatic reorganization relative to the disordered PE spacer layers. However, the data we obtained from the NP−film PNR suggest that the amine thiol layer changes similarly to the PE layers, increasing the NP−film separation distance at pH 2 and decreasing it at pH 12.

We propose two mechanisms that may contribute to the pH-induced modulation of the NP−film separation distance observed for the amine thiol SAM spacer layer. The first is that the PNR may be transducing differences in the relative affinity of the amine group toward the gold NPs at the different pH values. We assume here that the gold NPs associate directly with the amine groups of the SAM due to the known affinity of amine groups toward gold[42,43] and the propensity of the citrate anions on the gold NPs to be easily displaced by amine groups.[44] However, it is believed that protonated amine groups do not interact as strongly with gold surfaces due to their loss of the free electron pair upon protonation.[42,45] Thus, we hypothesize that at extremely low pH values the amines become fully protonated and start to lose their affinity toward the gold NPs, which may encourage the NPs to move away from the SAM and underlying gold film. As the pH increases, the amines become fully deprotonated, which causes a tighter association with the gold NPs and pulls the NPs toward the SAM and gold film. The second mechanism we propose for the observed pH-induced swelling of the amine thiol SAM, which seems more likely than the first proposed mechanism, is that the SAM itself reorganizes in response to pH changes due to protonation and deprotonation of the terminal amine groups. It is commonly accepted that when SAMs form, the thiol molecules assume some degree of tilt relative to the gold surface,[46,47] which represents a molecular arrangement with a minimum free energy. In the case of amine thiol SAMs, it is reasonable to expect that the packing and orientation of the molecules within the SAM depend on the charge state of the amine groups and that the SAM can reorganize slightly with changes in the charge state. The electrostatic reorganization of SAMs with charged terminal functional groups has been investigated in previous reports.[48−50] We suggest that when the amine thiol SAM is immersed in pH 2 solution, the SAM reorganizes slightly and effectively increases in thickness due to charge repulsion of the protonated, positively charged amine groups, and at pH 12, the SAM assumes a more compact configuration when the amines are fully deprotonated and uncharged.

CONCLUSIONS

The results presented herein are an important step forward in making the PNR technology more useful and accessible to researchers by adapting it for cuvette-based sensing studies that can be performed with standard spectrophotometers using T-LSPR spectroscopy. The distinctive feature of the platform we describe here relative to previous reports of T-LSPR measurements involving plasmonic coupling is that this NP−film system—instead of relying on the ability to form close-packed NP networks for adequate LSPR coupling response—simply uses single 60 nm NPs plasmonically coupled to a 30 nm film,

which produces uniformly aligned resonant dipoles that shift in wavelength very sensitively with subtle changes in NP−film separation distance. The coupled NP−film LSPR, and hence the precise NP−film separation distance, can be probed directly by T-LSPR measurements as long as the sample is placed at an angle relative to the illumination beam such that the NP−film axis is not parallel to the illumination beam and some degree of p-polarization is achieved. To enable high-throughput NP−film PNR studies that can be conducted in aqueous solutions, we used cuvette slide holders to place the NP−film PNR samples at an optimal angle relative to the collinear optical path defined by the spectrophotometer. This allows NP−film PNR samples to be immersed in various solutions in the cuvette and enables measurement of the response from millions of NP−film PNRs simultaneously by a single spectroscopic measurement from a standard UV−vis spectrophotometer. We calibrated the distance sensitivity of the T-LSPR mode NP−film PNR in water, which we used to suggest pH-induced angstrom-scale swelling and deswelling of PE spacer layers as thin as 1 PE layer and also from a thin amine-terminated SAM. The ability to perform very sensitive, high-throughput PNR measurements in aqueous solution on dynamically changing molecular spacer layers using a UV−vis spectrophotometer is a first step in the quest to design technologically simple sensors that take advantage of the exquisite distance sensitivity of the NP−film PNR.

METHODS

Molecular Spacer Layer Preparation. Gold films and the molecular spacer layers with attached gold nanoparticles were prepared and characterized similarly to our previously published articles.[8,17] Thin gold films of 30 nm were deposited in a class 100 clean room onto Nexterion Glass B slides ("clean room cleaned", Schott North America, Inc.) by an electron beam evaporator (CHA Industries) at 2 Å/s using a 5 nm chromium adhesion layer (deposited at 1 Å/s). Gold films were stored in 200 proof ethanol at 4 °C until use in experiments, as we have found previously that using more rigorous cleaning methods to completely remove all organic contaminants can have detrimental effects on our ability to produce good NP−film samples.[8] We use 30 nm gold films in this study as a compromise between our requirements of (1) maximizing the light transmission through the film and (2) producing a strong, coupled NP−film LSPR peak. We have found previously that 15 nm gold films produce a relatively weak and broadened coupled NP−film LSPR relative to 30 nm gold films. We avoid using films thicker than 30 nm because the 30 nm films produce an acceptable coupled NP−film response and adding thickness to the film would decrease the amount of light that can pass through the film, which would hinder T-LSPR NP−film measurements.

Polyelectrolyte spacer layers were prepared by layer-by-layer deposition[38,39] of poly(allylamine) hydrochloride (MW = 70 kDa, Aldrich) and polystyrenesulfonate (MW = 70 kDa, Aldrich). For each deposition step, the gold-coated glass slides were immersed in 0.003 mol-of-monomer/L PE and 1 M NaCl for 5 min, rinsed thoroughly with a gentle stream of ultrapure water (18 MΩ, used throughout), and immersed in fresh ultrapure water for 1 min, after which the substrates were either immersed in 1 M NaCl for 30 s before repeating the same steps for deposition of the oppositely charged PE or dried with a stream of high-purity nitrogen for analysis. No pH adjustments were made to the fabrication or rinse solutions. Solutions of PSS and PAH with 1 M NaCl were found to be pH 5.6 and 5.7, respectively. In the case of the NS-pH10 samples, the deposition procedure differed in that the solutions of PEs did not contain any additional NaCl and were adjusted to pH 10 using concentrated NaOH and sulfuric acid, and the brief NaCl rinse was replaced with a brief rinse in pH 10 water. All LBL depositions were initiated and terminated with the cationic PAH layer to facilitate both the attachment of the first PE layer to the gold film through amine−gold interactions[42,43] and the electrostatic immobilization of gold NPs to the PE spacer layer.

Self-assembled monolayers were fabricated on gold films using 11-amino-1-undecanethiol hydrochloride (referred to in this article as "C11 amine thiol", Sigma 674397, used as received). The SAMs were fabricated by incubating a gold slide in a clean glass vial containing a ∼2 mM thiol solution in 200 proof ethanol for 18 h. Following incubation, the vials containing the gold slides and thiol solutions were sonicated in a water bath at low power (power "4" out of "10" using a Crest Ultrasonics model 230D sonicator) for 2 min and then overflow rinsed with five reaction volumes of 200 proof ethanol. This sonication and rinsing step was performed a total of four times for each slide before removing the slide from the ethanol solution and drying it with a stream of high-purity nitrogen.

For most studies in this article, gold film samples were cut to size prior to deposition of molecular spacer layers and NPs. However, for the LBL calibration study, PE layers were deposited onto full gold film coated slides and then later cut into the pieces necessary to make dry and hydrated ellipsometry, spectroscopic reflectivity, and absorption measurements.

NP Deposition. Gold NPs (BBI) of 60 nm were electrostatically immobilized on each molecular spacer layer. Deposition of the gold NPs onto the PE layers was done by applying drops of the undiluted stock solution of gold NPs to each functionalized gold film for an incubation time of 30 min and then rinsing with ultrapure water and drying with a stream of high-purity nitrogen. This NP deposition results in 5−6 scatterers per μm^2, with 98% of them being single NPs on gold film (Supporting Information).

Ellipsometry. Molecular spacer layer thicknesses were characterized using a J.A. Woollam Co., Inc., M-88 variable-angle spectroscopic ellipsometer and WVASE32 software (version 3.460). Spectroscopic scans (277.5−763 nm) of each spacer layer were performed in three distinct regions of the functionalized gold films that did not contain immobilized NPs at 65°, 70°, and 75° relative to the normal of the surface of the slide. Ellipsometry data were analyzed using a two-layer model[51] composed of a bulk gold layer underneath an organic layer, which was used to represent the molecular layer. The thickness of each spacer layer was fitted using the Cauchy expression for normal dispersion[52] provided by the WVASE32 software using the default values for all parameters, including 1.45 for the parameter "*A*" representing the long wavelength asymptotic refractive index of the organic layer, such that the mean standard error of the fit was minimized. The nominal thickness of each spacer layer was determined to be the average of three independent thickness measurements of the spacer layer. The optical constants of the bare gold film were determined immediately prior to LBL deposition by spectroscopic scans of the bare gold films at 65°, 70°, and 75° and fitting n (refractive index) and k to the known values of bulk gold, which were provided by the WVASE32 software, to account for any shifts in the optical constants due to variation

dx.doi.org/10.1021/ph500190q | ACS Photonics 2014, 1, 974−984

in the thickness of the gold films. These fitted optical constants for each gold slide were saved and used later, respectively, when fitting for thickness of the molecular layers deposited onto the gold slides.

***In Situ* Ellipsometry.** Hydrated thicknesses of the PE spacer layers used in the LBL calibration study were measured using the same ellipsometry system described above in the Ellipsometry section. Inspired by liquid cell designs from Richter's group,[53,54] we fabricated a liquid cell by first creating a 3D printed mold (printed using a Stratasys Dimension 1200ES) to hold glass slides in place so as to create optical windows oriented to accept 70° illumination from the ellipsometer. The glass slides were then sealed to form a chamber with an open top using aquarium safe silicone sealant (see the Supporting Information for more detail). The WVASE32 software was used along with a silicon standard to calculate and account for the optical effects of the liquid cell on the ellipsometry measurements. With the cell in place, containing a sample and filled with water, thickness measurements were made similar to the dry state, but using only a 70° illumination angle. The thicknesses were fitted using the same model described above, but included a top ambient layer of water in the model.

NP−Film Plasmonic Characterization. Plasmonic properties of the NP−film samples were characterized by spectroscopic reflectivity and transmitted extinction measurements on dry and hydrated samples. Reflectivity spectra were acquired using the VASE instrument described above. Aside from the angle study presented in Figure 2D, all reflectivity spectra were collected using an illumination beam directed at 70° relative to the gold film surface normal. Integration time was controlled by the "Revs/Meas" variable in the WVASE32 software, which was kept constant at 400 for all reflectivity spectra. The illumination beam was provided by the xenon lamp included with the instrument and had a beam diameter of ∼4 mm. Dry samples were simply placed on the ellipsometer stage for measurement, and hydrated samples were placed inside of the water-filled ellipsometry liquid cell described above. The spectral range of this VASE instrument is limited, which is why the spectra appear to be cropped at 775 nm. This is simply an instrument limitation that we accepted due to the ease with which reflectivity spectra at various angles can be acquired using a VASE. Reflectivity spectra containing a wider wavelength range from similar NP−film samples than those present here can be seen in Mock et al.[17]

Transmitted extinction spectra were collected using a Cary 300 (Varian, Inc.) spectrophotometer equipped with a temperature controller. All spectra were collected at 25 °C using a 0.2 s/nm integration time. NP−film samples were inserted into standard size (1 cm path length) disposable plastic cuvettes containing custom slide holders that positioned the NP−film samples at various angles relative to the beam path of the instrument (Figure 2A−C). The NP−film samples were positioned so that the illumination beam first passed through the gold film (with immobilized NPs) and then through the supporting glass slide. The beam size at the sample was set using the spectral bandwidth software parameter of 2, which produced a beam ∼3 mm wide and ∼7 mm tall. The slide holders were designed using Autocad and 3D printed from ABSplus thermoplastic using a Stratasys uPrint SE Plus. After 3D printing and support removal, the slide holders were sonicated in ultrapure water containing sodium dodecyl sulfate for 1 h, soaked overnight in the same solution, and then thoroughly rinsed with ultrapure water before use. Aside from the angle study presented in Figure 2E, all extinction spectra were obtained using the 60° slide holders. Even though the NP−film LSPR peak is stronger in T-LSPR spectra acquired at greater illumination angles (Figure 2E), we used the 60° holder to ensure that the transmitted beam was not clipped by the width of the NP−film samples, which effectively narrows with respect to the collinear optical path as the illumination angle increases. Dry NP−film T-LSPR extinction spectra were obtained with samples mounted in the slide holders within cuvettes containing no water. Hydrated extinction spectra were acquired by simply adding water to the cuvette containing the slide holder and NP−film sample.

All NP−film sample spectra were normalized/baseline corrected to that of a gold film containing a corresponding molecular spacer layer and no immobilized NPs. This was done automatically by either the WVASE32 or the spectrophometer software through the acquisition of a blank spectrum. In the case of the spectrophotometer, the instrument was operated in double beam mode with the reference cell empty during sample acquisition.

Plasmon resonance peak positions were calculated by taking the centroid of top (or bottom in the case of reflectivity spectra where peaks are "dips") 50% of the resonances observed in either the transmitted extinction or the reflectivity curves. All of the NP−film spectra presented here represent the signal from millions of individual PNRs from each sample, and thus it was not necessary to take multiple spectra for each sample, as one would do if interrogating single PNRs on a sample one-by-one. The standard deviation from the population of PNRs on each sample is represented by the peak width of the NP−film LSPR and manifests itself in the calculation of the peak position through our use of the peak centroid to determine the peak position. For this reason, the data plots that show the NP−film LSPR or PNR measurement versus NP−film separation distance or pH do not have error bars.

pH-Induced Swelling Experiments. pH-induced swelling experiments were done using four separate cuvettes and 60° slide holders: two cuvettes for the sample and blank with pH 2 water and two cuvettes for the sample and blank with pH 12 water. We did this to minimize cross contamination during the pH cycling, as the 3D printed slide holders are slightly porous. The low-pH solution was ultrapure water with concentrated sulfuric acid added dropwise until the pH of the solution reach 2.1, which we call "pH 2" throughout the article. The high-pH solution was ultrapure water with concentrated NaOH added dropwise until the pH of the solution reached 11.8, which we call "pH 12" here. We measured refractive indices (Bellingham & Stanley model 340 refractometer) of the pH 2 and pH 12 solutions to be 1.332 76 and 1.332 73, respectively, which indicates that there was a negligible difference in refractive index between the solutions. Each pH swelling experiment was initiated by placing an NP−film sample and corresponding blank sample into the pH 2 cuvettes containing 3D printed slide holders and incubated for 30 min, after which the extinction spectrum was obtained using the spectrophotometer. Then the NP−film samples were removed from the cuvettes containing the pH 2 solutions and added to the cuvettes containing the pH 12 solutions. These cuvettes containing the samples were then rinsed three times with fresh pH 12 solution before starting the 30 min incubation at pH 12 and then acquiring the pH 12 sample spectra. This process was repeated for each sample until eight pH switches were obtained.

■ ASSOCIATED CONTENT

Supporting Information

Ellipsometry data, including a description of our *in situ* ellipsometry; images of representative NP−film samples; dry and hydrated reflectivity and T-LSPR NP−film spectra; dry and hydrated reflectivity and T-LSPR NP−film PNR calibration; data showing s-, p-, and unpolarized NP−film T-LSPR spectra; representative NP−film T-LSPR spectra from pH actuation studies; tabulated data from the pH swelling experiments; and data from an extended, 2-day 1L pH actuation study are included in the Supporting Information. This material is available free of charge via the Internet at http://pubs.acs.org.

■ AUTHOR INFORMATION

Corresponding Author

*E-mail: ryan.hill@duke.edu.

Present Address

[⊥]Department of Chemical Engineering, North Carolina State University, Raleigh, North Carolina, United States.

Notes

The authors declare no competing financial interest.

■ ACKNOWLEDGMENTS

We acknowledge Cristian Ciracì for theoretical discussions regarding the work presented here; Casey J. Galvin and Jan Genzer for insightful *in situ* ellipsometry discussion; Greg J. Nusz and Yu-Ju Tsai for developing the MATLAB code for finding centroids of plasmon resonance peaks; and Marcus H. Henderson and David F. Katz for use of their refractometer. This work was partially supported by NIH grant R01EB013896-01A1 and by the NSF's Research Triangle MRSEC (DMR-1121107). D.R.S. acknowledges partial support from the Air Force Office of Scientific Research (contract no. FA9550-09-1-0562).

■ REFERENCES

(1) Su, K.; Wei, Q.; Zhang, X.; Mock, J. J.; Smith, D. R.; Schultz, S. Interparticle Coupling Effects on Plasmon Resonances of Nanogold Particles. *Nano Lett.* **2003**, *3*, 1087−1090.

(2) Sönnichsen, C.; Reinhard, B. M.; Liphardt, J.; Alivisatos, A. P. A Molecular Ruler Based on Plasmon Coupling of Single Gold and Silver Nanoparticles. *Nat. Biotechnol.* **2005**, *23*, 741−745.

(3) Reinhard, B. M.; Siu, M.; Agarwal, H.; Alivisatos, A. P.; Liphardt, J. Calibration of Dynamic Molecular Rulers Based on Plasmon Coupling between Gold Nanoparticles. *Nano Lett.* **2005**, *5*, 2246−2252.

(4) Jain, P. K.; Huang, W.; El-Sayed, M. A. On the Universal Scaling Behavior of the Distance Decay of Plasmon Coupling in Metal Nanoparticle Pairs: A Plasmon Ruler Equation. *Nano Lett.* **2007**, *7*, 2080−2088.

(5) Skewis, L. R.; Reinhard, B. M. Spermidine Modulated Ribonuclease Activity Probed by RNA Plasmon Rulers. *Nano Lett.* **2008**, *8*, 214−220.

(6) Yang, L.; Wang, H.; Yan, B.; Reinhard, B. M. Calibration of Silver Plasmon Rulers in the 1− 25 nm Separation Range: Experimental Indications of Distinct Plasmon Coupling Regimes. *J. Phys. Chem. C* **2010**, *114*, 4901−4908.

(7) Guo, L.; Ferhan, A. R.; Chen, H.; Li, C.; Chen, G.; Hong, S.; Kim, D.-H. Distance-Mediated Plasmonic Dimers for Reusable Colorimetric Switches: A Measurable Peak Shift of More Than 60 Nm. *Small* **2012**, *9*, 234−240.

(8) Hill, R. T.; Mock, J. J.; Hucknall, A.; Wolter, S. D.; Jokerst, N. M.; Smith, D. R.; Chilkoti, A. Plasmon Ruler with Angstrom Length Resolution. *ACS Nano* **2012**, *6*, 9237−9246.

(9) Schultz, S.; Smith, D. R.; Mock, J. J.; Schultz, D. Single-Target Molecule Detection with Nonbleaching Multicolor Optical Immunolabels. *Proc. Natl. Acad. Sci. U.S.A.* **2000**, *97*, 996−1001.

(10) Wu, L.; Reinhard, B. M. Probing Subdiffraction Limit Separations with Plasmon Coupling Microscopy: Concepts and Applications. *Chem. Soc. Rev.* **2014**, *43*, 3884−3897.

(11) Park, S.-J.; Lazarides, A. A.; Storhoff, J.; Pesce, L.; Mirkin, C. A. The Structural Characterization of Oligonucleotide-Modified Gold Nanoparticle Networks Formed by DNA Hybridization. *J. Phys. Chem. B* **2004**, *108*, 12375−12380.

(12) Sebba, D. S.; Mock, J. J.; Smith, D. R.; Labean, T. H.; Lazarides, A. A. Reconfigurable Core-Satellite Nanoassemblies as Molecularly-Driven Plasmonic Switches. *Nano Lett.* **2008**, *8*, 1803−1808.

(13) Reinhard, B. M.; Sheikholeslami, S.; Mastroianni, A.; Alivisatos, A. P.; Liphardt, J. Use of Plasmon Coupling to Reveal the Dynamics of DNA Bending and Cleavage by Single Ecorv Restriction Enzymes. *Proc. Natl. Acad. Sci. U.S.A.* **2007**, *104*, 2667−2672.

(14) Chen, J. I. L.; Chen, Y.; Ginger, D. S. Plasmonic Nanoparticle Dimers for Optical Sensing of DNA in Complex Media. *J. Am. Chem. Soc.* **2010**, *132*, 9600−9601.

(15) Chen, J. I. L.; Durkee, H.; Traxler, B.; Ginger, D. S. Optical Detection of Protein in Complex Media with Plasmonic Nanoparticle Dimers. *Small* **2011**, *7*, 1993−1997.

(16) Ciracì, C.; Hill, R. T.; Mock, J. J.; Urzhumov, Y.; Fernández-Domínguez, A. I.; Maier, S. A.; Pendry, J. B.; Chilkoti, A.; Smith, D. R. Probing the Ultimate Limits of Plasmonic Enhancement. *Science* **2012**, *337*, 1072−1074.

(17) Mock, J. J.; Hill, R. T.; Tsai, Y.-J.; Chilkoti, A.; Smith, D. R. Probing Dynamically Tunable Localized Surface Plasmon Resonances of Film-Coupled Nanoparticles by Evanescent Wave Excitation. *Nano Lett.* **2012**, *12*, 1757−1764.

(18) Mock, J. J.; Hill, R. T.; Degiron, A.; Zauscher, S.; Chilkoti, A.; Smith, D. R. Distance-Dependent Plasmon Resonant Coupling between a Gold Nanoparticle and Gold Film. *Nano Lett.* **2008**, *8*, 2245−2252.

(19) Nath, N.; Chilkoti, A. A Colorimetric Gold Nanoparticle Sensor to Interrogate Biomolecular Interactions in Real Time on a Surface. *Anal. Chem.* **2002**, *74*, 504−509.

(20) Kalyuzhny, G.; Vaskevich, A.; Schneeweiss, M. A.; Rubinstein, I. Transmission Surface-Plasmon Resonance (T-Spr) Measurements for Monitoring Adsorption on Ultrathin Gold Island Films. *Chem. Eur. J.* **2002**, *8*, 3849−3857.

(21) Haes, A. J.; Van Duyne, R. P. A Nanoscale Optical Biosensor: Sensitivity and Selectivity of an Approach Based on the Localized Surface Plasmon Resonance Spectroscopy of Triangular Silver Nanoparticles. *J. Am. Chem. Soc.* **2002**, *124*, 10596−10604.

(22) Marinakos, S. M.; Chen, S.; Chilkoti, A. Plasmonic Detection of a Model Analyte in Serum by a Gold Nanorod Sensor. *Anal. Chem.* **2007**, *79*, 5278−5283.

(23) Kedem, O.; Tesler, A. B.; Vaskevich, A.; Rubinstein, I. Sensitivity and Optimization of Localized Surface Plasmon Resonance Transducers. *ACS Nano* **2011**, *5*, 748−760.

(24) Jia, K.; Bijeon, J. L.; Adam, P. M.; Ionescu, R. E. A Facile and Cost-Effective TEM Grid Approach to Design Gold Nano-Structured Substrates for High Throughput Plasmonic Sensitive Detection of Biomolecules. *Analyst* **2013**, *138*, 1015−1019.

(25) Driskell, J. D.; Lipert, R. J.; Porter, M. D. Labeled Gold Nanoparticles Immobilized at Smooth Metallic Substrates: Systematic Investigation of Surface Plasmon Resonance and Surface-Enhanced Raman Scattering. *J. Phys. Chem. B* **2006**, *110*, 17444−17451.

(26) Hill, R. T.; Mock, J. J.; Urzhumov, Y.; Sebba, D. S.; Oldenburg, S.; Chen, S.-Y.; Lazarides, A. A.; Chilkoti, A.; Smith, D. R. Leveraging Nanoscale Plasmonic Modes to Achieve Reproducible Enhancement of Light. *Nano Lett.* **2010**, *10*, 4150−4154.

(27) Mubeen, S.; Zhang, S.; Kim, N.; Lee, S.; Krämer, S.; Xu, H.; Moskovits, M. Plasmonic Properties of Gold Nanoparticles Separated from a Gold Mirror by an Ultrathin Oxide. *Nano Lett.* **2012**, *12*, 2088−2094.

(28) Tokarev, I.; Tokareva, I.; Minko, S. Optical Nanosensor Platform Operating in near-Physiological pH Range via Polymer-Brush-Mediated Plasmon Coupling. *ACS Appl. Mater. Interfaces* **2011**, *3*, 143−146.
(29) Le, F.; Lwin, N. Z.; Steele, J. M.; Käll, M.; Halas, N. J.; Nordlander, P. Plasmons in the Metallic Nanoparticle-Film System as a Tunable Impurity Problem. *Nano Lett.* **2005**, *5*, 2009−2013.
(30) Wanunu, M.; Popovitz-Biro, R.; Cohen, H.; Vaskevich, A.; Rubinstein, I. Coordination-Based Gold Nanoparticle Layers. *J. Am. Chem. Soc.* **2005**, *127*, 9207−9215.
(31) Tokareva, I.; Minko, S.; Fendler, J. H.; Hutter, E. Nanosensors Based on Responsive Polymer Brushes and Gold Nanoparticle Enhanced Transmission Surface Plasmon Resonance Spectroscopy. *J. Am. Chem. Soc.* **2004**, *126*, 15950−15951.
(32) Okamoto, T.; Yamaguchi, I. Optical Absorption Study of the Surface Plasmon Resonance in Gold Nanoparticles Immobilized onto a Gold Substrate by Self-Assembly Technique. *J. Phys. Chem. B* **2003**, *107*, 10321−10324.
(33) Bhat, R.; Genzer, J.; Chaney, B.; Sugg, H.; Liebmann-Vinson, A. Controlling the Assembly of Nanoparticles Using Surface Grafted Molecular and Macromolecular Gradients. *Nanotechnology* **2003**, *14*, 1145−1152.
(34) Lertvachirapaiboon, C.; Baba, A.; Ekgasit, S.; Thammacharoen, C.; Shinbo, K.; Kato, K.; Kaneko, F. Distance-Dependent Surface Plasmon Resonance Coupling between a Gold Grating Surface and Silver Nanoparticles. *Plasmonics* **2014**, *9*, 899−905.
(35) Jiang, G.; Baba, A.; Ikarashi, H.; Xu, R.; Locklin, J.; Kashif, K.; Shinbo, K.; Kato, K.; Kaneko, F.; Advincula, R. Signal Enhancement and Tuning of Surface Plasmon Resonance in Au Nanoparticle/Polyelectrolyte Ultrathin Films. *J. Phys. Chem. C* **2007**, *111*, 18687−18694.
(36) Itano, K.; Choi, J.; Rubner, M. F. Mechanism of the pH-Induced Discontinuous Swelling/Deswelling Transitions of Poly (Allylamine Hydrochloride)-Containing Polyelectrolyte Multilayer Films. *Macromolecules* **2005**, *38*, 3450−3460.
(37) Hiller, J. A.; Rubner, M. F. Reversible Molecular Memory and pH-Switchable Swelling Transitions in Polyelectrolyte Multilayers. *Macromolecules* **2003**, *36*, 4078−4083.
(38) Decher, G. Fuzzy Nanoassemblies: Toward Layered Polymeric Multicomposites. *Science* **1997**, *277*, 1232−1237.
(39) Tang, Z.; Wang, Y.; Podsiadlo, P.; Kotov, N. A. Biomedical Applications of Layer-by-Layer Assembly: From Biomimetics to Tissue Engineering. *Adv. Mater.* **2006**, *18*, 3203−3224.
(40) Huang, F. M.; Wilding, D.; Speed, J. D.; Russell, A. E.; Bartlett, P. N.; Baumberg, J. J. Dressing Plasmons in Particle-in-Cavity Architectures. *Nano Lett.* **2011**, *11*, 1221−1226.
(41) Dubas, S.; Schlenoff, J. Factors Controlling the Growth of Polyelectrolyte Multilayers. *Macromolecules* **1999**, *32*, 8153−8160.
(42) Michota, A.; Kudelski, A.; Bukowska, J. Molecular Structure of Cysteamine Monolayers on Silver and Gold Substrates: Comparative Studies by Surface-Enhanced Raman Scattering. *Surf. Sci.* **2002**, *502*, 214−218.
(43) Wallwork, M. L.; Smith, D. A.; Zhang, J.; Kirkham, J.; Robinson, C. Complex Chemical Force Titration Behavior of Amine-Terminated Self-Assembled Monolayers. *Langmuir* **2001**, *17*, 1126−1131.
(44) Sardar, R.; Shumaker-Parry, J. S. Asymmetrically Functionalized Gold Nanoparticles Organized in One-Dimensional Chains. *Nano Lett.* **2008**, *8*, 731−736.
(45) Kudelski, A.; Hill, W. Raman Study on the Structure of Cysteamine Monolayers on Silver. *Langmuir* **1999**, *15*, 3162−3168.
(46) Bain, C. D.; Troughton, E. B.; Tao, Y. T.; Evall, J.; Whitesides, G. M.; Nuzzo, R. G. Formation of Monolayer Films by the Spontaneous Assembly of Organic Thiols from Solution onto Gold. *J. Am. Chem. Soc.* **1989**, *111*, 321−335.
(47) Porter, M. D.; Bright, T. B.; Allara, D. L.; Chidsey, C. E. D. Spontaneously Organized Molecular Assemblies. 4. Structural Characterization of N-Alkyl Thiol Monolayers on Gold by Optical Ellipsometry, Infrared Spectroscopy, and Electrochemistry. *J. Am. Chem. Soc.* **1987**, *109*, 3559−3568.
(48) Osnis, A.; Sukenik, C.; Major, D. Structure of Carboxyl-Acid-Terminated Self-Assembled Monolayers from Molecular Dynamics Simulations and Hybrid Quantum Mechanics−Molecular Mechanics Vibrational Normal-Mode Analysis. *J. Phys. Chem. C* **2011**, *116*, 770−782.
(49) Lahann, J.; Mitragotri, S.; Tran, T.-N.; Kaido, H.; Sundaram, J.; Choi, I. S.; Hoffer, S.; Somorjai, G. A.; Langer, R. A Reversibly Switching Surface. *Science* **2003**, *299*, 371−374.
(50) Forster, R.; O'Kelly, J. pH Modulated Heterogeneous Electron Transfer across Metal/Monolayer Interfaces. *J. Phys. Chem.* **1996**, *100*, 3695−3704.
(51) Tronin, A.; Lvov, Y.; Nicolini, C. Ellipsometry and X-Ray Reflectometry Characterization of Self-Assembly Process of Polystyrenesulfonate and Polyallylamine. *Colloid Polym. Sci.* **1994**, *272*, 1317−1321.
(52) Cant, N.; Zhang, H.; Critchley, K.; Mykhalyk, T.; Davies, G.; Evans, S. Fabrication and Characterization of Self-Assembled Nanoparticle/Polyelectrolyte Multilayer Films. *J. Phys. Chem. B* **2003**, *107*, 13557−13562.
(53) Carton, I.; Brisson, A. R.; Richter, R. P. Label-Free Detection of Clustering of Membrane-Bound Proteins. *Anal. Chem.* **2010**, *82*, 9275−9281.
(54) Eisele, N. B.; Frey, S.; Piehler, J.; Görlich, D.; Richter, R. P. Ultrathin Nucleoporin Phenylalanine-Glycine Repeat Films and Their Interaction with Nuclear Transport Receptors. *EMBO Rep.* **2010**, *11*, 366−372.